The Turkish Journal of Pediatrics 2022; 64: 519-530
https://doi.org/10.24953/turkjped.2021.4600

Original Article

Pediatric head and neck rhabdomyosarcoma; the role of MRI in differentiation from other common pediatric malignant head and neck tumors

Şafak Parlak, Ekim Gümeler, Elif Bulut

Department of Radiology, Hacettepe University Faculty of Medicine, Ankara, Turkey.

ABSTRACT

Background. The tumor localization/extent and imaging characteristics of rhabdomyosarcomas (RMSs) especially parameningeal type, could overlap with the common tumors of the head and neck (H&N) such as lymphoma and nasopharyngeal carcinoma (NPC). Our goal was to investigate magnetic resonance imaging (MRI) features that could favor the diagnosis of RMS over lymphoma and NPC in H&N region.

Methods. Pretreatment MRI of 42 pediatric patients (mean: 9.7±5.1 years, min-max: 2-18 years) with a recent diagnosis of RMS (n=12), lymphoma (n=14) and NPC (n=16) were retrospectively studied. Tumor localization, extension and spread were evaluated. Signal and enhancement characteristics of the tumors and the presence of necrosis were noted. ADC values were measured by using both the small sample and single slice methods. For comparison of three groups, the Kruskal Wallis test and Pairwise comparisons were used. The intra-class correlation coefficient (ICC) was calculated for the assessment of inter-observer agreement.

Results. Nasopharynx ±parapharyngeal space involvement was detected in 58.3% of RMSs. Rhabdomyosarcoma was more heterogeneous in T2 images compared to lymphoma ($p=0.014$). Rhabdomyosarcoma showed significantly higher frequency of heterogeneous enhancement ($p<0.001$) and necrosis ($p<0.001$) among these tumors. The mean ADC values of lymphoma were significantly lower than the values of RMS ($p<0.001$) and NPC ($p<0.01$) for both observers. The mean ADC values were higher in RMSs than NPCs ($p>0.05$). Intra-class correlation in ADC measurements was higher for the single slice method (ICC=0.997) than the small sample method (ICC=0.989).

Conclusions. Rhabdomyosarcoma tends to have higher ADC values than lymphoma and has a higher frequency of heterogeneous enhancement and necrotic parts than both lymphoma and nasopharyngeal carcinoma. These features could help radiologists to differentiate RMS from the above-mentioned mimickers.

Key words: rhabdomyosarcoma, nasopharyngeal carcinoma, lymphoma, diffusion-weighted imaging, magnetic resonance imaging.

Rhabdomyosarcoma (RMS), as one of the small blue round cell tumors (SBRCTs), is the most common sarcoma of childhood representing 50.9% of all.[1] It is the second most common head and neck (H&N) malignancy after lymphoma in the pediatric age.[2] Rhabdomyosarcoma has a slight male predominance and is usually diagnosed before the age of 10 years; it can also affect older children.[1,3,4] It has embryonic, alveolar, pleomorphic and spindle cell/sclerosing subtypes.[5] The embryonic subtype affects younger patients and has a good prognosis whereas the alveolar subtype affects older children and has a poor prognosis.[3] The pleomorphic subtype is seen only in adults. Spindle cell/sclerosing subtype is rare and most commonly involves paratesticular and H&N regions.[6]

Head and neck RMSs could be divided into subgroups according to the primary location

✉ Şafak Parlak
parlaksafak@gmail.com

Received 16th September 2021, revised 29th November 2021, 13th January 2022, accepted 24th January 2022.

such as parameningeal, nonparameningeal, and orbital RMSs.[7,8] Parameningeal RMSs arise in regions adjacent to the meninges such as the nasopharynx, parapharyngeal space, masticatory space, nasal/paranasal regions.[8] Therefore, parameningeal RMSs harbor surgical difficulties and have a poor outcome. Non-parameningeal RMSs tend to be superficial.[8,9]

Signal characteristics of RMS in magnetic resonance imaging (MRI) are not specific; demonstrating intermediate to high signal intensity (SI) on T2 weighted images (WI) and intermediate SI on T1WI compared to muscle.[9] Head and neck RMSs may show various enhancement patterns; most are reported to enhance heterogeneously.[10] Non-enhancing areas corresponding to necrosis or hemorrhage may be seen.[8,10] Similar to other SBRCTs including lymphoma, RMS demonstrates restricted diffusion due to high cellularity.[11-13]

The imaging characteristics of RMSs, especially parameningeal type, could overlap with the common tumors of the H&N region such as lymphoma and nasopharyngeal carcinoma (NPC) including restriction of diffusion.[8-10]

The definition of the site of origin and the differentiation of RMS is not frequently problematic when it is localized in striated muscles with distortion of the adjacent tissues. Nevertheless, RMS originates from primitive mesenchymal cells and it can arise anywhere where striated muscle is not normally found.[1] Furthermore, RMSs generally rapidly grow with adjacent tissue infiltration[14,15] and sometimes it can be difficult to clearly discriminate the tissue compartments on MRI and thus differentiate RMSs using generally known MRI features. Distinguishing these tumors, which is important for determining different treatment management, can be difficult because of the overlapping demographics, tumor location and extent, and imaging features. Our goal was to investigate imaging discriminators that could favor the diagnosis of RMSs over lymphoma and NPC.

Material and Methods

Patients

Institutional Review Board (2020/16-26) approved the study protocol and informed consent was waived by Hacettepe University Institutional Review Board. A retrospective research was performed from July 2014 to June 2020 in Hospital Information System to identify patients with histopathologically proven diagnosis of RMS, lymphoma and NPC. Inclusion criteria were as follows: 1) patients younger than 18 years old; 2) histopathologically proven diagnosis of RMS, suprahyoid lymphoma and NPC; 3) patients with an MRI scan before biopsy and treatment. Exclusion criteria were as follows: 1) orbital lesions (mainly affecting orbits); 2) too small masses with the longest diameter < 1cm on axial T2WI, to ensure an appropriate localization of region of interest (ROI); 3) images with prominent distortion or susceptibility artifacts; 4) MR examination in which diffusion-weighted imaging was not performed.

Imaging

All MR examinations were performed on 1.5 T scanners (Achieva, Philips Healthcare, Best, the Netherlands; Signa, GE Healthcare, Milwaukee, Wisconsin; and Symphony, Siemens, Erlangen, Germany). The imaging protocol was the same for all scans and included coronal, sagittal, and axial T1WI, coronal short tau inversion recovery (STIR) image, axial T2WI with fat saturation, single shot echo planar imaging (EPI) DWI and post-contrast fat-saturated axial and coronal T1WI. Imaging parameters were; T1WI (TR/TE: 410-640/7-15 ms, 3.5-4 mm section thickness, NEX: 1-2, FA: 90°), coronal STIR (TR/TE: 2353-6200/37-60 ms, 3.5-4 mm section thickness, NEX: 1-2, FA: 90°), axial fat-saturated T2WI (TR/TE: 2320-5000/83-90 ms, 3-4 mm section thickness, NEX: 1-2, FA: 90°), DWI (TR/TE: 3400-5674/75-94 ms, and 3-4 mm section thickness, NEX: 2-4, FA: 90°). Post-contrast T1W images were obtained after IV injection of 0.1 mmol/kg gadolinium-based contrast agent.

Single-shot echo-planar imaging (SS-EPI) technique was used for DWI acquisition and performed before the contrast media injection. DWI was acquired with three b-value with values of 0, 500, and 1000 s/mm^{-2}. Apparent diffusion coefficient (ADC) maps were automatically generated.

Image Evaluation

Qualitative Analysis was performed on hospital Picture Archiving and Communication System (PACS) in consensus by two neuroradiologists (SP and EB, 4- and 7-year experience in H&N radiology) blinded to histopathologic diagnosis. Tumor localization and affected spaces were noted. If more than one space were infiltrated by the tumor, involvement was defined as multicompartment involvement. The presence of skull base invasion, intracranial extension, and retropharyngeal and/or cervical lymphadenopathy were also noted. Distant organ metastasis/involvement was determined by cross-sectional imaging (CT, MRI and PET-CT) findings.

Signal characteristics and post-contrast enhancement patterns of tumors were evaluated. Tumor necrosis was defined as the presence of high SI on T2WI, low SI on T1WI, lack of enhancement with high ADC levels.[10,16,17]

The quantitative analysis was performed on hospital PACS independently by two neuroradiologists (SP and EB) blinded to histopathologic diagnosis. ADCs of the tumors were measured by using both the small sample and single slice method. In the small sample method, three separate circular ROI's (with an area of 1cm^2) were placed on the darkest area on ADC maps, which probably represent the highest cellular activity within the tumor. The necrotic areas were avoided. The mean values obtained from these measurements were defined as ADC_{lesion}. In the single slice method, a freehand ROI was drawn outlining the largest cross-sectional area of the tumor (ADC_{area}) from a single slice.

Statistics Analysis

IBM Statistics 23.0 was used for statistical analysis and the *p* value of <0.05 was considered significant. Categorical variables were presented as count and percentage. Mean and standard deviations (SD) and median (Min-Max) values were given for variables with normal distribution and without normal distribution, respectively. For comparison of three groups, the Kruskal Wallis test was used. Pairwise comparisons were made to determine the relationship between groups. The intra-class correlation coefficient (ICC) was calculated for the assessment of inter-observer agreement. In terms of agreement, ICC value was interpreted as poor (< 0.50), moderate (0.50-0.75), good (0.75-0.90), or excellent (>0.90).

Results

The study included 12 patients with RMS (9 parameningeal and 3 nonparameningeal), 14 patients with lymphoma and 16 patients with NPC. A flow chart of the patients enrolled in the study is shown in Figure 1. Seven patients (58.3%) had embryonic, two patients (16.7%) had spindle cell/sclerosing and one patient (8.3%) had alveolar histopathologic subtypes of RMS. In two patients with RMS histopathologic subtype was undetermined.

Demographic features of the patients, tumor localization and extent, signal and enhancement characteristics are summarized in Table I.

The median age of patients with NPC was significantly higher than the median age of patients with RMS and lymphoma (p<0.001 and p=0.002) There was no significant difference between RMS and lymphoma cohorts on age (p>0.05).

Multicompartment involvement was frequent in both NPC (seen in all cases) and RMS (75%) cohorts. Nasopharyngeal carcinoma showed significantly more multicompartment involvement than lymphoma (p=0.003) and RMS

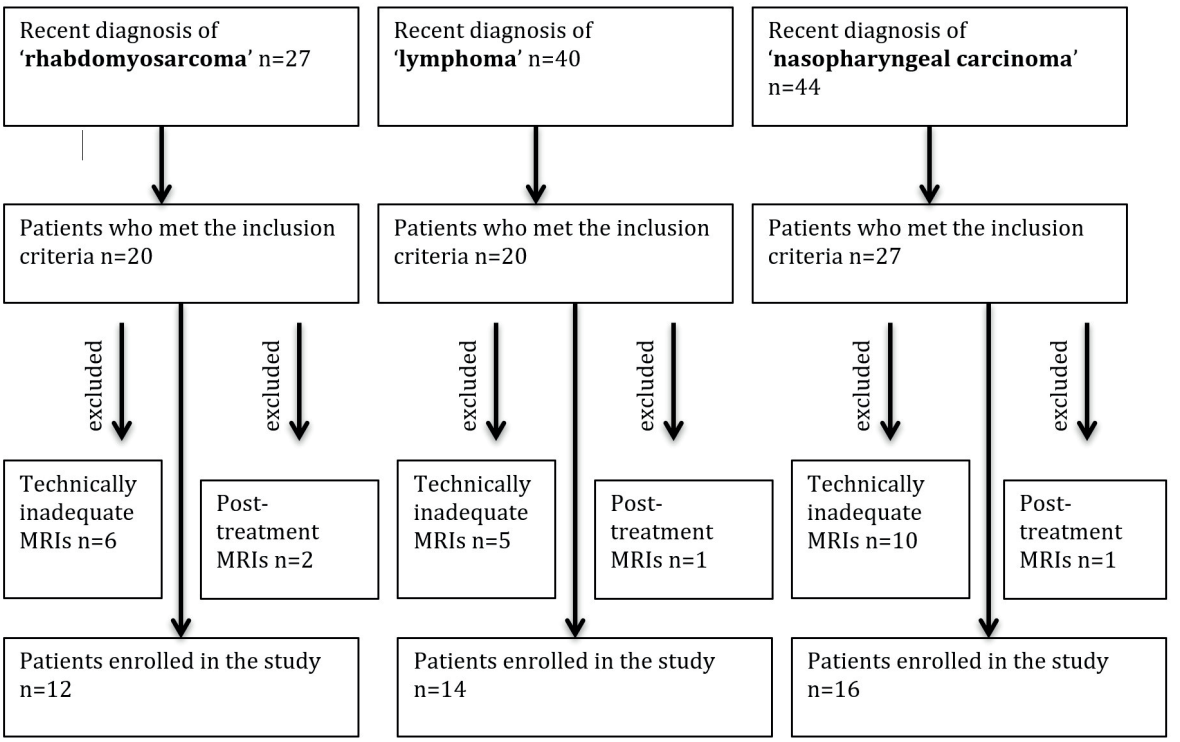

Fig. 1. Flow chart of the patients enrolled in the study.

(p=0.034). There was no significant difference between RMS and lymphoma in terms of multicompartment involvement (p=0.34).

Nasopharyngeal ±parapharyngeal involvement was found as 58.3% in RMS and 57.1% in lymphoma (Fig. 2). Skull base involvement, cervical and retropharyngeal lymphadenopathy were more common in patients with NPC (p<0.001 and p<0.05). In three RMS cases (25%) and in four lymphoma cases (28.6%) tumors tend to encircle vascular structures.

Distant organ metastasis/involvement was seen in five lymphoma patients (p=0.014). Five patients had intraabdominal lymphadenopathy (35.7%), four patients had splenic involvement (28.5%), three patients had hepatic involvement (21%), two patients had intrathoracic lymphadenopathy (14%), two patients had bone marrow involvement (14%). Kidney (n=1), pancreas (n=1) and axillary lymph nodes (n=1) were rare involvement areas.

T2 signal homogeneity was significantly more common in lymphoma (p<0.01). RMS was more heterogeneous in T2 images compared to lymphoma (p=0.014). RMS and NPC were not different in terms of T2 homogeneity (p>0.05). RMS lesions showed a significantly higher ratio of heterogeneous enhancement than lymphoma and NPC (p<0.001). A total of seven patients (six embryonic and one spindle cell/sclerosing subtypes) with RMS (58.3%) had imaging findings compatible with tumor necrosis. None of the lymphoma and NPC had necrotic component (p<0.001) (Fig. 3).

The mean values of ADC_{lesion} and ADC_{area} for each group and the results of the Kruskal Wallis test are summarized in Table II. The mean ADC values were significantly different between groups (p≤0.001).

Through further evaluation with pairwise comparisons, the mean ADC values (ADC_{lesion} and ADC_{area}) were found to be significantly

Table I. Summary of demographics, pathologic and imaging characteristics.

	RMS *n:12*	Lymphoma *n:14*	Nasopharyngeal ca. *n:16*	*p* value
Gender (F/M)	5/7	1/13	2/14	0.088
Median age (years) (min-max)	4 (2-17)	7 (2-15)	14 (11-18)	<0.001*
Multicompartment involvement	75% n:9	57.1% n:8	100% n:16	0.008*
Nasopharynx±parapharyngeal involvement	58.3% n:7	57.1% n:8	100% n:16	0.004*
Skull base involvement	58.3% n:7	35.7% n:5	93.7% n:15	<0.001*
Intracranial extension	8.3% n:1	14.2% n:2	31.2% n:5	0.332
Distant metastasis/distant organ involvement	-	35.7% n:5	-	0.014*
Lymphadenopathy (cervical/retropharyngeal)	41.7% n:5	57.1% n:8	93.7% n:15	0.018*
T2 signal intensity				
Homogeneous	16.7% n:2	64.3% n:9	18.8% n:3	0.006*
Heterogeneous	83.3% n:10	35.7% n:5	81.2% n:13	
Enhancement[a]				
Homogeneous	16.7% n:2	78.6% n:11	81.2% n:13	<0.001*
Heterogeneous	83.3% n:10	21.4% n:3	12.5% n:2	
Presence of necrosis	58.3% n:7	0% n:0	0% n:0	<0.001*

[a] Post-contrast T1WI was not available in a nasopharyngeal carcinoma patient.
*Statistically significance
RMS: Rhabdomyosarcoma

Table II. The comparison of ADC measurements of groups with Kruskal-Wallis Test.

	Rhabdomyosarcoma		Lymphoma		Nasopharyngeal ca.		*p* value	
	Obs1	Obs2	Obs1	Obs2	Obs1	Obs2	Obs1	Obs2
Mean ADC_{lesion} ($x10^{-3}mm^2/s$)	0.907±0.2	0.891±0.21	0.481±0.08	0.456±0.14	0.687±0.11	0.683±0.11	<0.001*	<0.001*
Mean ADC_{area} ($x10^{-3}mm^2/s$)	1.125±0.37	1.135±0.35	0.517±0.08	0.528±0.08	0.740±0.12	0.747±0.15	<0.001*	<0.001*

Values are expressed as mean±SD.
*Statistically significance
Obs1:Observer 1; Obs2: Observer 2

lower in lymphoma than the means of RMS ($p<0.001$ for both observers) and the means of NPC (for ADC_{lesion} $p=0.004$ for obs1; $p=0.001$ for obs2 and for ADC_{area} $p=0.003$ for obs1; $p=0.008$ for obs2) (Fig. 4). The mean values of ADC_{lesion} ($p=0.13$ for obs1; $p=0.21$ for obs2) and ADC_{area} ($p=0.07$ for obs1; $p=0.06$ for obs2) did not show a significant difference between RMS and NPC.

Inter-observer agreement in ADC measurements was higher for the single slice method (ICC=0.997) than the small sample method (ICC=0.989).

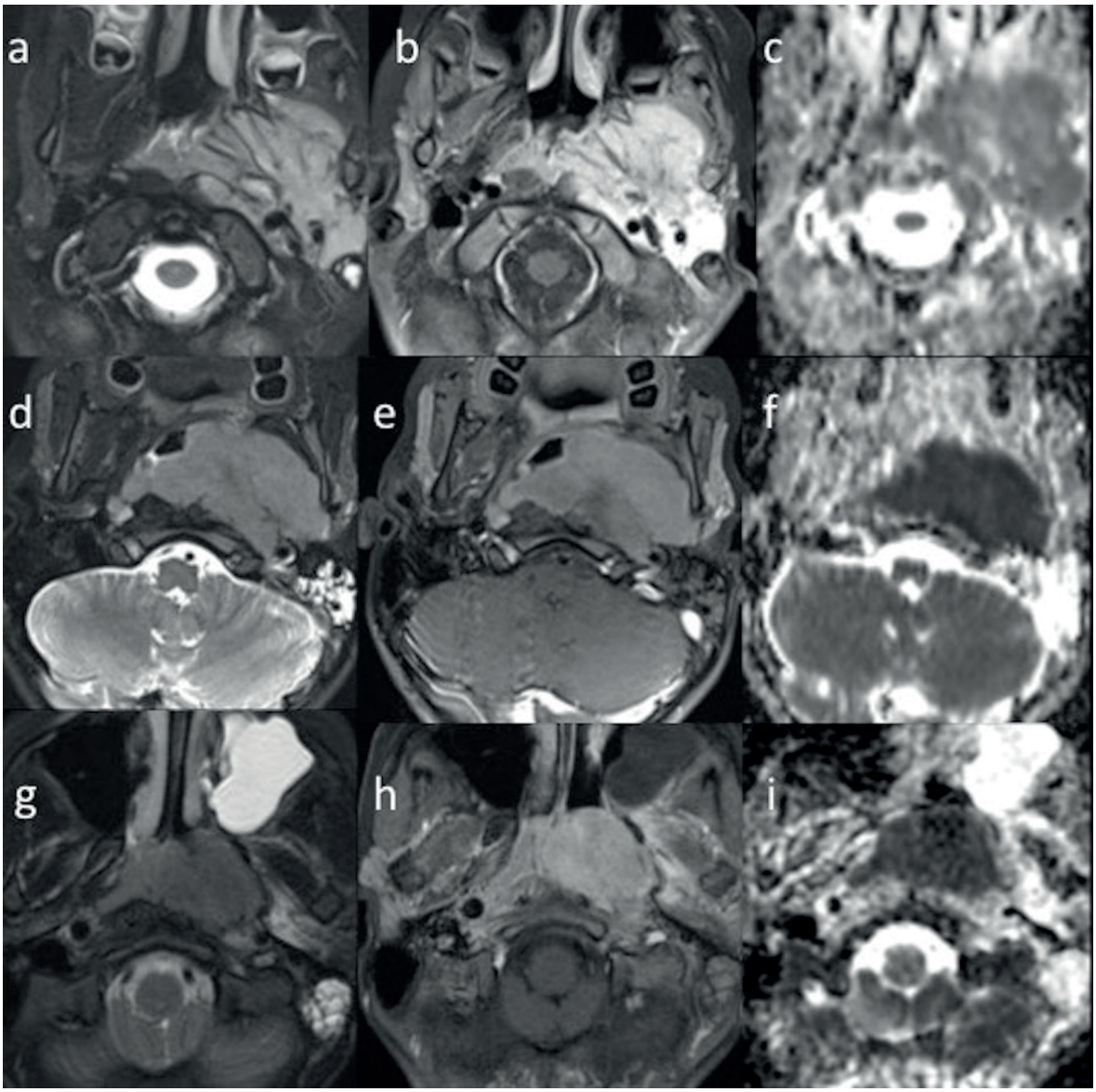

Fig. 2. The MRIs of 6-year-old male patient with RMS (a-c), 12-year-old male patient with lymphoma (d-f) and 13-year-old male patient with nasopharyngeal carcinoma (g-i) with nasopharyngeal and parapharyngeal extension. There is no apparent difference in terms of signal and enhancement characteristics on fat-sat T2WI (a, d, g), and post-contrast fat-sat T1WI (b, e, h). RMS (c) shows higher signal intensity on ADC map compared to lymphoma (f) and nasopharyngeal carcinoma (i).

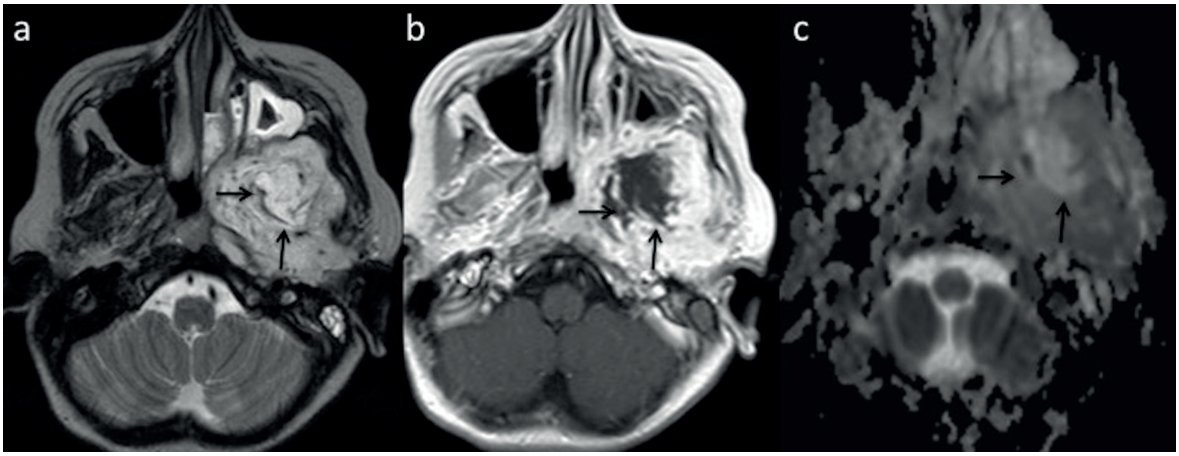

Fig. 3. A 10-year-old female patient with RMS. Necrosis within tumor appears as T2 hyperintense area with lack of enhancement and diffusion restriction (arrows).

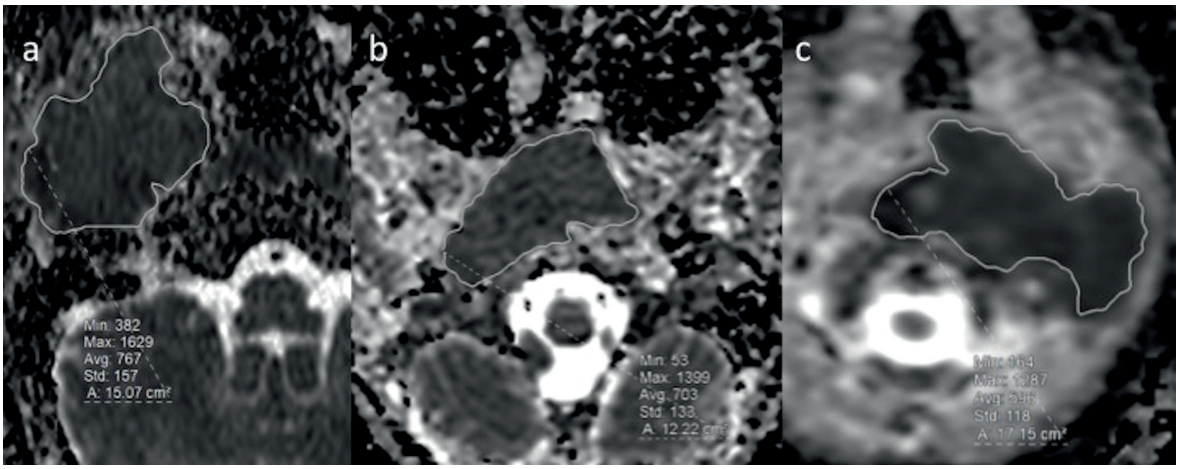

Fig. 4. ADC measurement of the tumors by single slice method; a) 8-year-old male patient with RMS (ADC_{area}: $0.76x10^{-3}$ mm^2/s). b) 15-year-old male patient with nasopharynx carcinoma (ADC_{area}: $0.70x10^{-3}$ mm^2/s). c) 3-year-old male patient with lymphoma (ADC_{area}: $0.59x10^{-3}$ mm^2/s).

Discussion

Parameningeal RMS has overlapping findings with lymphoma and NPC in terms of tumor localization and extent.[9] Nasopharyngeal ±parapharyngeal involvement was frequent in both RMS (58.3%) and lymphoma (57.1%) in our study. Further complicating differential diagnosis, previously reported MRI findings of RMS including high T2 signal intensity, prominent enhancement and restricted diffusion are also seen in the other tumors of concern.[9] To our knowledge, there is no previous study comparing MRI characteristics of these three tumors in the literature. In our study, we found a significant difference in terms of ADC values between RMS and lymphoma; in terms of enhancement pattern and presence of necrosis between RMS and lymphoma or NPC. These imaging findings could be used to help distinguish RMS and could guide effective management of these patients.

The age distribution (median age: 4 years) and a slight male predominance in our RMS cohort were compatible with the literature.[3,4] Although the median age of patients with RMS was significantly smaller than the median age of patients with NPC, there was an overlap between the two cohorts in older ages. The most

common pathologic subtype was embryonic RMS, compatible with the age distribution.

Rhabdomyosarcoma has a locally invasive behavior that is reflected by our high rates of multicompartment involvement (75%) and lack of distant metastasis. Treatment of RMS depends on the histologic subtype, tumor location and stage. It mainly utilizes a multimodality approach that includes systemic chemotherapy and local therapy; consisting of surgery, radiation therapy, or both on a case-by-case basis.[18] Although frequently seen in patients with NPC, skull base involvement was less commonly encountered in RMS (58.3%). In the presence of skull base involvement and intracranial extension, treatment options differ and survival becomes poorer.[19,20] The intracranial extension was rare in RMS (8.3%) and detected more frequently in patients with NPC, although there was no significant difference between the two groups. Cervical and retropharyngeal lymphadenopathies were significantly more frequent in NPC; distant metastasis was seen in lymphoma. These findings could be used adjunctively with the other imaging findings for tumor discrimination.

The signal homogeneity on T2WI was a common finding (%64.3) in lymphoma compared to RMS and NPC (p=0.006). This finding is compatible with the imaging characteristics of sinonasal lymphoma described previously in literature like the other findings in our lymphoma cohort such as frequent homogeneous enhancement (n=11, 78.6%) and lack of necrosis.[21,22] T2 signal heterogeneity and heterogeneous enhancement in pediatric RMS due to necrosis or hemorrhage were also reported previously.[10,23,24] These two findings were frequently detected in our group of RMS (83.3%) and heterogeneous enhancement was significantly more common than both NPC and lymphoma that could be used as a valuable imaging discriminator to favor the diagnosis of RMS.

Tumor necrosis is characterized by the presence of dead cells with preservation of the tissue architecture. It is reported to be an important hallmark of aggressive tumors and associates with hypoxia and angiogenesis.[25,26] In our study, neither lymphoma nor NPC showed necrotic parts despite RMS lesions (58.3%). In literature, embryonal RMS was noted to be more homogeneous with a lower rate of necrosis than alveolar and pleomorphic subtypes.[27] Our findings could be attributed due to the size of the embryonal tumors, because almost all (83.3%) presented as large tumors with multicompartment involvement. Additionally, our small-sized cohort has limitations to reflect the general behavior of this histopathologic type.

Diffusion-weighted imaging is efficiently used to differentiate between benign and malignant H&N tumors and helps in avoiding unnecessary invasive diagnostic procedures or surgery.[11,13,28] In high-grade malignant neoplasms, ADC values are generally low due to high mitotic activity, increase in cell number and size, decrease in the cytoplasm and extracellular matrix. Several studies particularly performed on adults reported that DWI is useful to distinguish lymphoma from NPC.[12,29-31] Our results were compatible; the lymphoma lesions had significantly lower ADC values compared to the NPC and RMS lesions. Since RMS usually presents as a rapidly progressing high-grade tumor, low ADC values could be expected. There are a few studies with a small number of patients that analyzed DWI characteristics of H&N RMSs in literature.[13,28] The ADC values of RMSs in those studies were reported to range from $0.66x10^{-3}$ mm^2/s to $0.91x10^{-3}$ mm^2/s. In the study with the largest number of RMS (n=11) among them, the mean ADC values were found to be $0.78\pm0.07x10^{-3}$ mm^2/s.[13] This value is notably lower than the mean ADC values measured by using the single slice ROI method in our RMS cohort ($1.125\pm0.37x10^{-3}$ mm^2/s for obs1, $1.135\pm0.35x10^{-3}$ mm^2/s for obs2) probably due to differences in the methods of measurement. In that study, the ROIs were placed in a single slice avoiding necrotic areas in contrary to our study in which single slice ROIs were drawn in the largest cross-sectional

area of the tumor including necrotic parts. The contribution of necrotic parts with high ADC values is considered to be responsible for higher ADC values in our RMS cohort measured by the single slice ROI method. The mean ADC values measured with the small sample method in our RMS cohort ($0.907\pm0.20x10^{-3}$ mm^2/s for obs1 and 0.891 ± 0.21 $x10^{-3}$ mm^2/s for obs2) are slightly higher than the mean value reported in that study.

In addition to the single slice method, the mean ADC values measured by the small sample method avoiding necrotic parts were also significantly higher in our RMS cohort compared to lymphoma. This probably reflects the histopathologic features of the embryonic type of RMS that was the most common type in our study. Embryonal RMS contains variable cellularity ranging from poorly differentiated primitive mesenchymal cells to highly differentiated muscle cells within a myxoid matrix.[32] The increasing effect of myxoid matrix on ADC in soft tissue tumor was previously reported.[33] Therefore, higher ADC values detected even in the non-necrotic areas of RMS could be explained by the myxoid matrix of the embryonal type.

Although no statistically significant difference was found, the mean ADC_{area} values have a tendency to be higher in RMS than NPC in our cohorts. This again probably reflects the presence of necrotic parts commonly found in RMS in contrast to NPC. The small size of our cohorts could be the reason for the difference not being statistically significant between the ADC values of these two tumors. Future studies with larger cohorts are recommended for further evaluation.

Long acquisition time, motion artifacts, and frequent need for general anesthesia are the main difficulties of MRI in pediatric patients. Besides, susceptibility artifacts are commonly encountered in DWI of the H&N region due to excessive air-tissue and tissue-bone interfaces. This may affect the correct localization of ROI and estimation of ADC values. ROI method may also affect the ADC measurements; the small sample ROI method has been reported to yield the worst inter-observer correlation in previous studies concerning thyroid nodules[34] and orbital tumors.[35] Our study supports previous reports; the ADC values measured with the single-slice ROI method showed higher inter-observer correlation than the ones measured with the small sample method. Additionally, the single-slice and whole-volume ROI methods are more representative of the histopathologic characteristics of tumors than the small sample ROI method. This is especially important in the discrimination of tumors like RMS with heterogeneous tissue characteristics due to necrosis/cysts or hemorrhage from more homogenous mimickers.

Although relatively small number of the patients with RMS (n=12) is a limitation, our RMS cohort presents the largest RMS series in the literature. The study has also some limitations due to its retrospective design; the scans were acquired using different scanners with different parameters, which could affect image evaluation. We believe the use of different scanners is not a major limitation. However, possible effect of using different scanners on ADC values cannot be completely excluded and more investigation is needed to make a definite assessment.

The data on which specific gadolinium-based contrast agent was used in the studies could not be found. On the other hand, we believe the use of different contrast agents is not a limitation for qualitative evaluation of enhancement patterns (whether homogenous or heterogeneous).

We also could not perform whole-volume ADC histogram analysis due to the software unavailability. Even though this method has a promising ability to predict histopathologic characteristics of lesions, its application is limited in clinical practice. Another limitation due to the retrospective design was the inability to histopathologically confirm necrotic parts defined in MRIs.

In conclusion, RMS tends to have higher ADC values than lymphoma and has a higher frequency of heterogeneous enhancement and necrotic parts than both lymphoma and NPC. These features could help radiologists to differentiate RMS from the above-mentioned mimickers. Future studies with larger cohorts are recommended to validate these findings.

Ethical approval

Institutional Review Board (2020/16-26) approved the study protocol and informed consent was waived by Hacettepe University Institutional Review Board.

Author contribution

The authors confirm contribution to the paper as follows: study conception and design: ŞP, EB; data collection: ŞP, EG, EB; analysis and interpretation of results: ŞP, EG, EB; draft manuscript preparation: ŞP, EG, EB. All authors reviewed the results and approved the final version of the manuscript.

Source of funding

The authors declare the study received no funding.

Conflict of interest

The authors declare that there is no conflict of interest.

REFERENCES

1. Miller RW, Young JL Jr, Novakovic B. Childhood cancer. Cancer 1995; 75(1 Suppl): 395-405. https://doi.org/10.1002/1097-0142(19950101)75:1+<395::AID-CNCR2820751321>3.0.CO;2-W
2. Sengupta S, Pal R. Clinicopathological correlates of pediatric head and neck cancer. J Cancer Res Ther 2009; 5: 181-185. https://doi.org/10.4103/0973-1482.57123
3. Oberlin O, Rey A, Lyden E, et al. Prognostic factors in metastatic rhabdomyosarcomas: results of a pooled analysis from United States and European cooperative groups. J Clin Oncol 2008; 26: 2384-2389. https://doi.org/10.1200/JCO.2007.14.7207
4. Raney RB, Meza J, Anderson JR, et al. Treatment of children and adolescents with localized parameningeal sarcoma: experience of the Intergroup Rhabdomyosarcoma Study Group protocols IRS-II through -IV, 1978-1997. Med Pediatr Oncol 2002; 38: 22-32. https://doi.org/10.1002/mpo.1259
5. Fletcher CDM, Bridge JA, Hogendoorn PCW, Mertens F, editors. WHO classification of tumours of soft tissue and bone. Lyon: IARC Press; 2013.
6. Agaram NP, LaQuaglia MP, Alaggio R, et al. MYOD1-mutant spindle cell and sclerosing rhabdomyosarcoma: an aggressive subtype irrespective of age. A reappraisal for molecular classification and risk stratification. Mod Pathol 2019; 32: 27-36. https://doi.org/10.1038/s41379-018-0120-9
7. Lloyd C, McHugh K. The role of radiology in head and neck tumours in children. Cancer Imaging 2010; 10: 49-61. https://doi.org/10.1102/1470-7330.2010.0003
8. Freling NJ, Merks JH, Saeed P, et al. Imaging findings in craniofacial childhood rhabdomyosarcoma. Pediatr Radiol 2010; 40: 1723-1738; quiz 855. https://doi.org/10.1007/s00247-010-1787-3
9. Jawad N, McHugh K. The clinical and radiologic features of paediatric rhabdomyosarcoma. Pediatr Radiol 2019; 49: 1516-1523. https://doi.org/10.1007/s00247-019-04386-5
10. Inarejos Clemente EJ, Navallas M, Barber Martínez de la Torre I, et al. MRI of Rhabdomyosarcoma and Other Soft-Tissue Sarcomas in Children. Radiographics 2020; 40: 791-814. https://doi.org/10.1148/rg.2020190119
11. Humphries PD, Sebire NJ, Siegel MJ, Olsen OE. Tumors in pediatric patients at diffusion-weighted MR imaging: apparent diffusion coefficient and tumor cellularity. Radiology 2007; 245: 848-854. https://doi.org/10.1148/radiol.2452061535
12. Razek AA. Diffusion-weighted magnetic resonance imaging of head and neck. J Comput Assist Tomogr 2010; 34: 808-815. https://doi.org/10.1097/RCT.0b013e3181f01796
13. Abdel Razek AA, Gaballa G, Elhawarey G, Megahed AS, Hafez M, Nada N. Characterization of pediatric head and neck masses with diffusion-weighted MR imaging. Eur Radiol 2009; 19: 201-208. https://doi.org/10.1007/s00330-008-1123-6

14. Nangalia R, Shah N, Sheikh MA, Pal M. Rhabdomyosarcoma involving maxilla mimicking gingival enlargement: a diagnostic challenge. BMJ Case Rep 2019; 12: e230692. https://doi.org/10.1136/bcr-2019-230692

15. Panta P, Felix D. Rhabdomyosarcoma: a rapidly growing malignancy. Pan Afr Med J 2015; 22: 121. https://doi.org/10.11604/pamj.2015.22.121.7479

16. Beddy P, Genega EM, Ngo L, et al. Tumor necrosis on magnetic resonance imaging correlates with aggressive histology and disease progression in clear cell renal cell carcinoma. Clin Genitourin Cancer 2014; 12: 55-62. https://doi.org/10.1016/j.clgc.2013.07.006

17. Razek AA, Megahed AS, Denewer A, Motamed A, Tawfik A, Nada N. Role of diffusion-weighted magnetic resonance imaging in differentiation between the viable and necrotic parts of head and neck tumors. Acta Radiol 2008; 49: 364-370. https://doi.org/10.1080/02841850701777390

18. Bradley JA, Kayton ML, Chi YY, et al. Treatment approach and outcomes in ınfants with localized rhabdomyosarcoma: a report from the soft tissue Sarcoma Committee of the Children's Oncology Group. Int J Radiat Oncol Biol Phys 2019; 103: 19-27. https://doi.org/10.1016/j.ijrobp.2018.08.017

19. Buwalda J, Schouwenburg PF, Blank LE, et al. A novel local treatment strategy for advanced stage head and neck rhabdomyosarcomas in children: results of the AMORE protocol. Eur J Cancer 2003; 39: 1594-602. https://doi.org/10.1016/S0959-8049(03)00363-0

20. Yang A, Wickremesekera A, Parker A, Davis C. Surgical management of craniofacial and skull base rhabdomyosarcomas. J Craniofac Surg 2009; 20: 1388-93. https://doi.org/10.1097/SCS.0b013e3181b187bb

21. Chen Y, Wang X, Li L, Li W, Xian J. Differential diagnosis of sinonasal extranodal NK/T cell lymphoma and diffuse large B cell lymphoma on MRI. Neuroradiology 2020; 62: 1149-1155. https://doi.org/10.1007/s00234-020-02471-3

22. Kim SH, Mun SJ, Kim HJ, Kim SL, Kim SD, Cho KS. Differential diagnosis of sinonasal lymphoma and squamous cell carcinoma on CT, MRI, and PET/CT. Otolaryngol Head Neck Surg 2018; 159: 494-500. https://doi.org/10.1177/0194599818770621

23. Agrons GA, Wagner BJ, Lonergan GJ, Dickey GE, Kaufman MS. From the archives of the AFIP. Genitourinary rhabdomyosarcoma in children: radiologic-pathologic correlation. Radiographics 1997; 17: 919-937. https://doi.org/10.1148/radiographics.17.4.9225391

24. Kobi M, Khatri G, Edelman M, Hines J. Sarcoma botryoides: MRI findings in two patients. J Magn Reson Imaging 2009; 29: 708-712. https://doi.org/10.1002/jmri.21670

25. Bredholt G, Mannelqvist M, Stefansson IM, et al. Tumor necrosis is an important hallmark of aggressive endometrial cancer and associates with hypoxia, angiogenesis and inflammation responses. Oncotarget 2015; 6: 39676-39691. https://doi.org/10.18632/oncotarget.5344

26. Edwards JG, Swinson DE, Jones JL, Muller S, Waller DA, O'Byrne KJ. Tumor necrosis correlates with angiogenesis and is a predictor of poor prognosis in malignant mesothelioma. Chest 2003; 124: 1916-1923. https://doi.org/10.1378/chest.124.5.1916

27. Allen SD, Moskovic EC, Fisher C, Thomas JM. Adult rhabdomyosarcoma: cross-sectional imaging findings including histopathologic correlation. AJR Am J Roentgenol 2007; 189: 371-377. https://doi.org/10.2214/AJR.07.2065

28. Abdel Razek AA, Nada N. Role of diffusion-weighted MRI in differentiation of masticator space malignancy from infection. Dentomaxillofac Radiol. 2013; 42: 20120183. https://doi.org/10.1259/dmfr.20120183

29. Fong D, Bhatia KS, Yeung D, King AD. Diagnostic accuracy of diffusion-weighted MR imaging for nasopharyngeal carcinoma, head and neck lymphoma and squamous cell carcinoma at the primary site. Oral Oncol 2010; 46: 603-606. https://doi.org/10.1016/j.oraloncology.2010.05.004

30. Lian S, Zhang C, Chi J, Huang Y, Shi F, Xie C. Differentiation between nasopharyngeal carcinoma and lymphoma at the primary site using whole-tumor histogram analysis of apparent diffusion coefficient maps. Radiol Med 2020; 125: 647-653. https://doi.org/10.1007/s11547-020-01152-8

31. Ozgen B, Oguz KK, Cila A. Diffusion MR imaging features of skull base osteomyelitis compared with skull base malignancy. AJNR Am J Neuroradiol 2011; 32: 179-184. https://doi.org/10.3174/ajnr.A2237

32. Parham DM, Barr FG. Classification of rhabdomyosarcoma and its molecular basis. Adv Anat Pathol 2013; 20: 387-397. https://doi.org/10.1097/PAP.0b013e3182a92d0d

33. Nagata S, Nishimura H, Uchida M, et al. Diffusion-weighted imaging of soft tissue tumors: usefulness of the apparent diffusion coefficient for differential diagnosis. Radiat Med 2008; 26: 287-295. https://doi.org/10.1007/s11604-008-0229-8

34. Zhou X, Ma C, Wang Z, et al. Effect of region of interest on ADC and interobserver variability in thyroid nodules. BMC Med Imaging 2019; 19: 55. https://doi.org/10.1186/s12880-019-0357-x

35. Xu XQ, Hu H, Su GY, Liu H, Shi HB, Wu FY. Diffusion weighted imaging for differentiating benign from malignant orbital tumors: diagnostic performance of the apparent diffusion coefficient based on region of interest selection method. Korean J Radiol 2016; 17: 650-656. https://doi.org/10.3348/kjr.2016.17.5.650